

# Entropy spectroscopy of a bilayer graphene quantum dot

C. Adam,<sup>1,\*</sup> H. Duprez,<sup>1</sup> N. Lehmann,<sup>1</sup> A. Yglesias,<sup>1</sup> S. Cances,<sup>1</sup> M. J. Ruckriegel,<sup>1</sup> M. Masseroni,<sup>1</sup> C. Tong,<sup>1</sup> A. O. Denisov,<sup>1</sup> W. Huang,<sup>1</sup> D. Kealhofer,<sup>1</sup> R. Garreis,<sup>1</sup> K. Watanabe,<sup>2</sup> T. Taniguchi,<sup>3</sup> K. Ensslin,<sup>1</sup> and T. Ihn<sup>1</sup>

<sup>1</sup>*Solid State Physics Laboratory, ETH Zurich, Zurich CH-8093, Switzerland*

<sup>2</sup>*Research Center for Electronic and Optical Materials,  
National Institute for Materials Science, 1-1 Namiki, Tsukuba 305-0044, Japan*

<sup>3</sup>*Research Center for Materials Nanoarchitectonics,  
National Institute for Materials Science, 1-1 Namiki, Tsukuba 305-0044, Japan*

(Dated: December 25, 2024)

We measure the entropy change of charge transitions in an electrostatically defined quantum dot in bilayer graphene. Entropy provides insights into the equilibrium thermodynamic properties of both ground and excited states beyond transport measurements. For the one-carrier regime, the obtained entropy shows that the ground state has a two-fold degeneracy lifted by an out-of-plane magnetic field. This observation is in agreement with previous direct transport measurements and confirms the applicability of this novel method. For the two-carrier regime, the extracted entropy indicates a non-degenerate ground state at zero magnetic field, contrary to previous studies suggesting a three-fold degeneracy. We attribute the degeneracy lifting to the effect of Kane-Mele type spin-orbit interaction on the two-carrier ground state, which has not been observed before. Our work demonstrates the validity and efficacy of entropy measurements as a unique, supplementary experimental tool to investigate the degeneracy of the ground state in quantum devices build in materials such as graphene. This technique, applied to exotic systems with fractional ground state entropies, will be a powerful tool in the study of quantum matter.

## I. INTRODUCTION

The thermodynamic entropy of a system is used to study the degeneracy of the quantum mechanical ground state of exotic phases of condensed matter. The non-abelian fractional quantum Hall state at filling factor  $5/2$  [1–3], Majorana fermions [4] and multi-channel Kondo systems [5] are predicted to exhibit fractional entropy specific to the respective quasiparticles constituting the phase. For these highly engineered systems, accessing the entropy with conventional methods such as used for bulk systems, e.g. measurements of heat capacity, is experimentally challenging [6]. Therefore, indirect schemes have been implemented to measure the entropy of mesoscopic systems, such as extracting the entropy from thermoelectric transport measurements [7]. An approach exploiting thermodynamic Maxwell relations [8, 9] has already been experimentally demonstrated for a localized spin-1/2 electron in an electrostatically defined quantum dot (QD) in a (Al)GaAs heterostructure. It has been further developed to measure the entropy of a Kondo spin-singlet [10, 11], and another thermodynamic quantity: the analogue to the magnetic susceptibility of a spin impurity in a ‘charge’ Kondo circuit [12].

Extending this technique to graphene multilayer systems is particularly attractive, as these have been shown to host a variety of exotic electronic phases, such as correlated insulators, the anomalous quantum Hall effect, and superconductivity [13–19]. However, only few studies report on measurements of thermodynamic quantities in

graphene systems as they often involve highly specialized measurement techniques [20, 21]. On the other hand, the entropy-to-charge conversion, pioneered in ref. [8], which requires to controllably define a charge island (with a charging energy substantially larger than the thermal energy) connected to a thermal bath, is accessible through standard transport measurements across a charge detector. This scheme is particularly suited to rhombohedral graphene systems in which gate-defined devices can be formed thanks to the bandgap opening with a transverse displacement field [22–25]. Here, we demonstrate such capacitance-based entropy measurements in a dual-gated (rhombohedral or Bernal) bilayer graphene (BLG) quantum dot, an object typically studied for semiconducting qubit purposes [26–28]. We measured the entropy change upon changing the quantum dot’s charge state. For a weakly-coupled dot to the reservoir, the entropy is directly connected to the charge ground state degeneracy. Notably, we measured that the ground state degeneracy of the second charge carrier is lower than expected, supported by excited state spectroscopy. We propose a model to explain this surprising behavior.

## II. DEVICE & EXPERIMENTAL SETUP

The schematic of the system is shown in Fig. 1(a). It consists of a QD in thermal equilibrium with a bath of hole carriers (“reservoir”), and a charge detection circuit (“detector”). A current  $I_{\text{heater}}$  is driven through electrostatically defined constrictions called heaters. The ohmic resistance of the heaters causes power to be dissipated as heat. This induces a temperature change of the reservoir due to Joule heating [29].

\* adamc@phys.ethz.ch

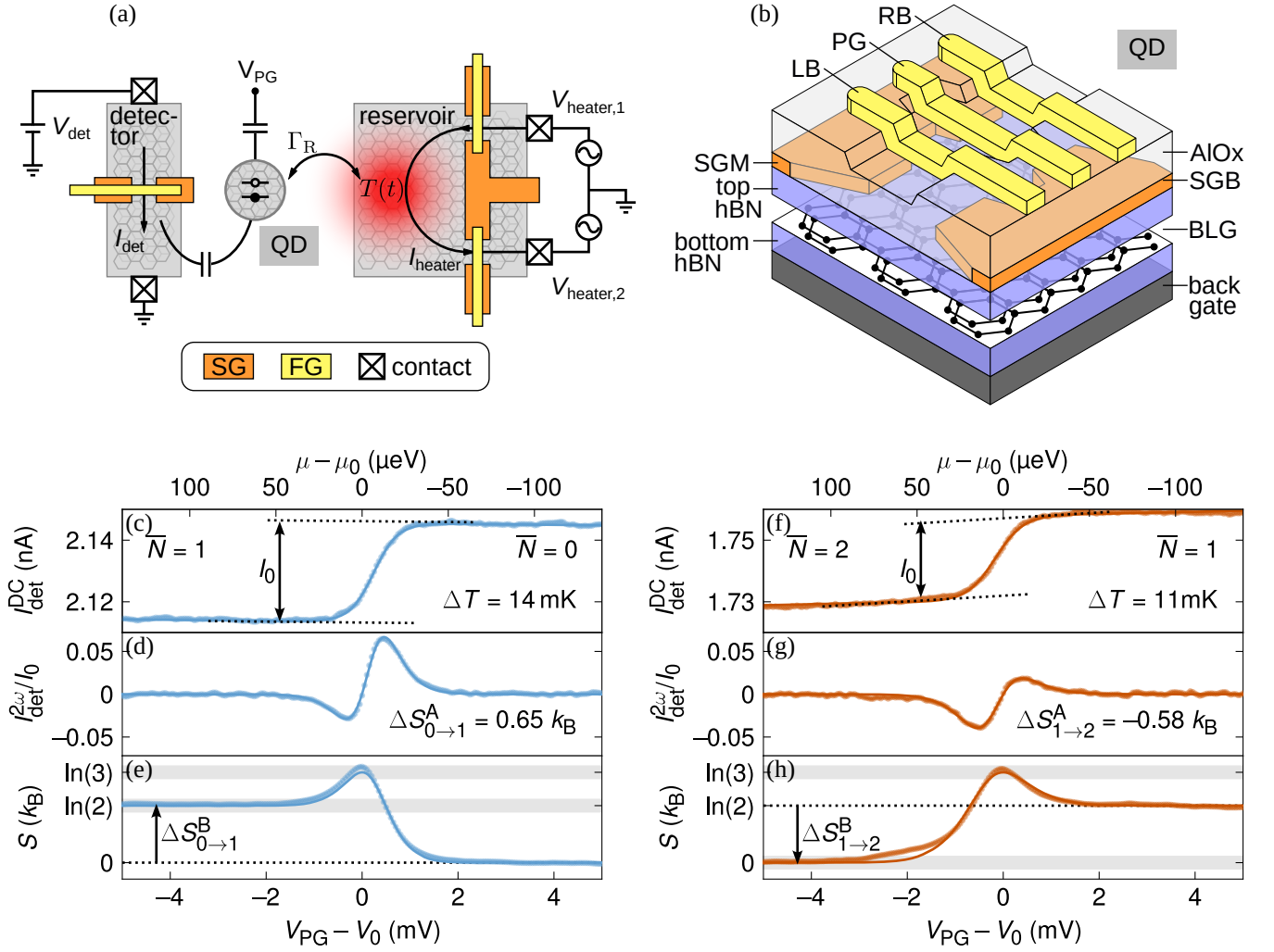


FIG. 1. (a) The sample consists of a quantum dot (QD) thermally coupled to a reservoir. The reservoir temperature  $T(t)$  is changed by driving a current  $I_{\text{heater}}$  through a heater structure defined by split gates (SG) and finger gates (FG). The charge detector (CD), capacitively coupled to the QD, carries a current  $I_{\text{det}}$  which changes as the number of charge carriers changes on the QD. (b) Schematic of the van der Waals (vdW) stack in the region of the QD: bilayer graphene (BLG) is encapsulated between two layers of hexagonal boron nitride (hBN) as dielectric. To form a conduction channel, the graphite back gate, BG, and gold split gates, SGM and SGB, are used to open a band gap and tune the hole carrier density in the BLG to deplete it of charge carriers underneath the gates. The finger gates, LB, PG, RB, are separated from the split gates by an aluminum oxide layer (AlOx) and used to define the tunnel barriers and tune the QD. For the  $0 \rightarrow 1^-$  and  $1 \rightarrow 2^-$  transition, respectively: The DC component of the detector current (c) and (f) with the extracted temperature modulation (continuous traces are fits to eq. 5), the to  $I_0$  normalized second harmonic current (d) and (g) with extracted entropy change (continuous traces are fits to eq. 6), and the entropy obtained by integration (e) and (h) (continuous traces are plots of eq. D14 in (e) and eq. D18 in (h)). The gray bars  $\pm 0.1 \ln(2)$  as a guide to the eye.

Fig. 1(b) shows a schematic side view of the van der Waals (vdW) stack in which the QD is defined: BLG is encapsulated by hexagonal boron nitride (hBN) surrounded by a global graphite back gate (BG) and with two layers of gold top gates: split gates SGM, SGB to form a one-dimensional channel, and finger gates to form the QD (plunger gate PG and tunneling barrier gates LB, RB). The top gate layers are separated by aluminum oxide (AlOx) as a dielectric. The displacement field is roughly  $-0.46 \text{ V/nm}$  resulting in a band gap of approximately  $50 \text{ meV}$ [30]. The device is operated

in the hole conduction regime. The barriers are tuned such that there is no coupling to the left lead. A more detailed description of the sample and its operation can be found in Appendix A.

### III. ENTROPY EXTRACTION

The relevant thermodynamic state variables of the QD-reservoir system include the mean occupation num-

ber  $N$  and entropy  $S$  of the QD, as well as the electrochemical potential  $\mu$  and carrier temperature  $T$  in the reservoir. In our experiment,  $\mu$  and  $T$  are independent, externally controlled variables. In an experiment conducted at constant temperature  $\bar{T}$ , these variables are connected through the Maxwell relation

$$S(\mu, \bar{T}) - S(\mu_0, \bar{T}) = \int_{\mu_0}^{\mu} \left( \frac{\partial \bar{N}(\mu, \bar{T})}{\partial T} \right)_{\mu} d\mu. \quad (1)$$

By measuring  $(\partial \bar{N} / \partial T)_{\mu}$  one can get the entropy of the system. In order to measure this quantity, we control the temperature  $T(t)$  by driving an electrical current

$$I_{\text{heater}}(t) = I_{\text{heater}} \cdot \cos(\omega t) \quad (2)$$

through the heaters. The temperature resulting from Joule heating can be expressed as [29]

$$T(t) = \sqrt{T_0^2 + aI_{\text{heater}}^2(t)} \quad (3)$$

$$\approx T_0 + \Delta T + \Delta T \cos(2\omega t), \quad (4)$$

where  $T_0$  is the reservoir temperature without any heating current and  $a$  is a system-specific constant which is determined by a calibration measurement. The average temperature increases to  $\bar{T} = T_0 + \Delta T$ , while a temperature modulation  $\Delta T = aI_{\text{heater}}^2 / 4T_0$  with frequency  $2\omega$  is introduced. The frequency  $\omega$  is chosen sufficiently low to ensure that the QD is in equilibrium with the reservoir at all times. The charge detector (CD) capacitively coupled to the QD [31] allows us to extract the mean occupation number  $\bar{N}$  via the detector current

$$I_{\text{det}}(t) \approx \overbrace{I_0 \cdot \bar{N}(\mu, \bar{T}) + I_{\text{off}} + \gamma V_{\text{PG}}}^{I_{\text{det}}^{\text{DC}}} \quad (5)$$

$$+ \underbrace{I_0 \cdot \left( \frac{\partial \bar{N}}{\partial T} \right)_{\mu, T=\bar{T}} \Delta T \cdot \cos(2\omega t)}_{I_{\text{det}}^{2\omega}} \quad (6)$$

where  $I_0$  is the change in CD current in response to a charge change on the QD,  $I_{\text{off}}$  the offset current through the CD at the operation point,  $V_{\text{PG}}$  the plunger gate voltage used to change the QD occupation, and  $\gamma$  the transconductance of the CD with respect to the plunger gate. The DC component  $I_{\text{det}}^{\text{DC}}$  is used to determine  $I_0$ , while the second harmonic component  $I_{\text{det}}^{2\omega}$  provides  $(\partial \bar{N} / \partial T)_{\mu, T=\bar{T}}$ , once  $\Delta T$  has been determined by calibration. The entropy difference  $\Delta S_{N-1 \rightarrow N}$  between the integer charge states  $N-1$  and  $N$  is obtained in two different ways.

**Method A:** In the thermally broadened regime, i.e.  $k_{\text{B}}T(t) \gg \Gamma_{\text{R}}$  with  $\Gamma_{\text{R}}$  characterizing the tunnel broadening, the QD occupation close to a transition between integer numbers  $N-1$  and  $N$  of charge carriers in the

QD is then described by

$$\bar{N}(\mu, \bar{T}) = \frac{1}{1 + e^{\frac{\mu_N - \mu - \bar{T} \Delta S_{N-1 \rightarrow N}}{k_{\text{B}} \bar{T}}}} + N - 1, \quad (7)$$

$$\left( \frac{\partial \bar{N}}{\partial T} \right)_{\mu, T=\bar{T}} = \frac{\frac{\mu_N - \mu - \Delta S_{N-1 \rightarrow N}}{4k_{\text{B}} \bar{T}^2}}{\cosh^2 \left( \frac{\mu_N - \mu - \bar{T} \Delta S_{N-1 \rightarrow N}}{2k_{\text{B}} \bar{T}} \right)}. \quad (8)$$

where  $\mu_N - \mu = \alpha_{\text{PG}} e(V_{\text{PG}} - V_0)$  and  $\mu_N$  is the electrochemical potential of the quantum dot for adding the  $N$ -th charge carrier,  $\alpha_{\text{PG}} \approx 0.025$  is the plunger gate lever arm, and  $V_0$  is a plunger gate voltage offset. Note that changing  $\mu$  in eqs. 7, 8 is equivalent to changing the energy difference  $\mu_N - \mu$ , which is accomplished in the experiment by changing  $V_{\text{PG}}$ . The measurements for obtaining  $\alpha_{\text{PG}}$  are shown in Appendix C. Eq. 8 contains  $\Delta S_{N-1 \rightarrow N}$  as a parameter. Since  $I_{\text{det}}^{2\omega} \propto (\partial \bar{N} / \partial T)_{\mu, T=\bar{T}}$  one can simply fit eq. 8 to  $I_{\text{det}}^{2\omega}$  and obtain  $\Delta S_{N-1 \rightarrow N}$ . This can be done without performing a temperature calibration.

**Method B:** Eq. 6 allows to get  $(\partial \bar{N} / \partial T)_{\mu, T=\bar{T}}$  from  $I_{\text{det}}^{2\omega}$ , without assumptions about its functional shape. However,  $I_0$  and  $\Delta T$  have to be known.  $I_0$  can be read from  $I_{\text{det}}^{\text{DC}}$  as shown in Fig. 1(c),(f).  $\Delta T$  is set by the heating current  $I_{\text{heater}}$  and calibrated in the beginning. After obtaining  $(\partial \bar{N} / \partial T)_{\mu, T=\bar{T}}$  one can get the entropy by using eq. 1. The integration along  $\mu$  is equivalent to an integration along  $V_{\text{PG}}$ , knowing  $\alpha_{\text{PG}}$ .

#### IV. ONE- & TWO-CARRIER ENTROPY

Fig. 1(c)-(e) show the measured charge detector current and extracted entropy for the transition between the  $0 \rightarrow 1$  charge state. The DC component of the detector current  $I_{\text{det}}^{\text{DC}}$  and the second harmonic component  $I_{\text{det}}^{2\omega}$  are measured with a voltmeter and lock-in amplifier attached to a transimpedance amplifier. The resulting traces are obtained by scanning the  $0 \rightarrow 1$  transition several times and averaging the individual traces. The changing plunger gate  $V_{\text{PG}}$  corresponds to an effective change of the electrochemical potential  $\mu$  of the reservoir by  $\Delta\mu = -\alpha_{\text{PG}} e(V_{\text{PG}} - V_0)$ . As the vacuum state  $|0\rangle$  is non-degenerate, we define the entropy to be  $S(N=0) = 0$ . Gradually changing the hole occupation number to  $N=1$  by lowering  $V_{\text{PG}}$ , the entropy reaches a maximum of  $k_{\text{B}} \ln(3)$  before settling at  $k_{\text{B}} \ln(2)$ . The entropy change for the  $0 \rightarrow 1$  transition is therefore  $\Delta S_{0 \rightarrow 1} = k_{\text{B}} \ln(2)$ . This can be understood based on the energy level structure of the one-carrier charge state: Its ground state is the Kramers pair  $|K^- \downarrow\rangle$ ,  $|K^+ \uparrow\rangle$ , hence two-fold degenerate at zero magnetic field. The result confirms observations recently made by performing counting statistics measurements on BLG QDs [32]. The entropy peak at  $k_{\text{B}} \ln(3)$  corresponds to the QD being equally likely in any of the following three microstates:

for  $N = 0$  this is the empty state  $|0\rangle$ , and for  $N = 1$  this is the two-fold degenerate Kramers pair  $|K^- \downarrow\rangle, |K^+ \uparrow\rangle$ .

Figures 1(f)-(g) show the measured results for the  $1 \rightarrow 2$  charge carrier transition. Starting out at  $N = 1$  with the initial entropy  $k_B \ln(2)$ , gradually changing the occupation number to  $N = 2$  by further lowering  $V_{PG}$ , the entropy has a maximum with  $k_B \ln(3)$  before settling at  $S(N = 2) = 0$ . The entropy change for the  $1 \rightarrow 2$  transition is therefore  $\Delta S_{1 \rightarrow 2} = -k_B \ln(2)$ . We conclude from this result that the ground state for  $N = 2$  particles in the QD is non-degenerate. This result is surprising as previous devices studied in higher magnetic fields suggested a valley-singlet spin-triplet ground state with a three-fold spin-degeneracy, a conclusion reached by extrapolating finite bias measurements to zero magnetic field [33, 34]. In our experiment, the entropy peak at  $k_B \ln(3)$  corresponds to the QD being equally likely in any of the microstates of  $N = 1$  (two microstates, Kramers pair) and  $N = 2$  (only one microstate), corresponding in total to three microstates of equal probability  $1/3$ . In Sec. V we study the change of entropy in magnetic field and from that provide a possible explanation for the lifting of degeneracy at zero magnetic field for the second charge carrier state.

Fig. 2 (a) shows the mean temperature  $\bar{T}$  of the hole bath forming the reservoir as a function of the heater current  $I_{\text{heater}}$ . Temperatures for individual heater currents are obtained by tuning the QD into the thermally

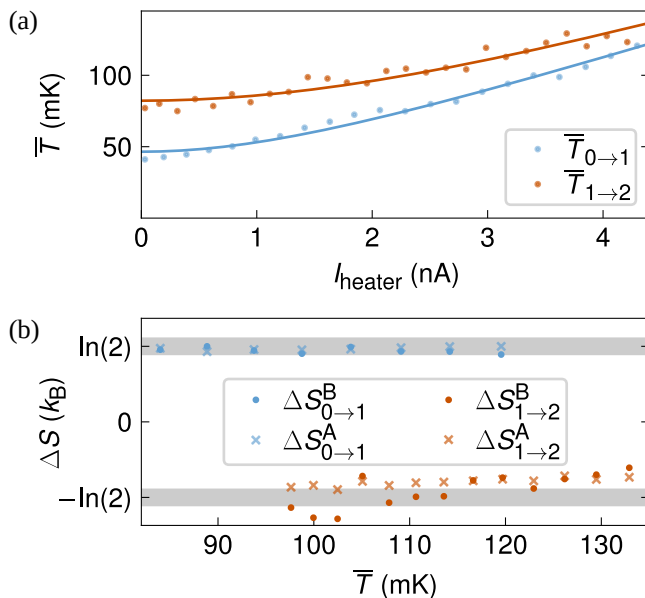


FIG. 2. (a) Average temperatures  $\bar{T}$  of the holes tunneling onto the QD as a function of the heater current  $I_{\text{heater}}$  for the  $0 \rightarrow 1$ - and  $1 \rightarrow 2$ -transition, respectively. The solid lines show a fit with eq. 3. The temperature at zero heating currents differ as the experiments where carried out at different cryostat base temperatures. (b) Entropy changes for the  $0 \rightarrow 1$  and  $1 \rightarrow 2$  transitions obtained using Method A and B. The results of both transitions are in reasonable agreement.

broadened regime and fitting eq.5 to  $I_{\text{det}}^{\text{DC}}$ . The evolution of  $\bar{T}$  in  $I_{\text{heater}}$  follows eq. 3 as can be seen from the fit. The experiments for the  $0 \rightarrow 1$  and  $1 \rightarrow 2$  transition were carried out at different cryostat temperatures  $T_0$ . The data is well described by eq. 3. From Fig. 2 (a) the temperature modulation  $\Delta T = \bar{T} - T_0$  is extracted for various heater currents. Fig. 2 (b) shows the entropy changes  $\Delta S_{0 \rightarrow 1}$ ,  $\Delta S_{1 \rightarrow 2}$  obtained by applying method A and B. Both methods show reasonable agreement with each other.

## V. ENTROPY IN MAGNETIC FIELD

Figures 3(a) and (b) show the entropy changes  $\Delta S_{0 \rightarrow 1}^A$  and  $\Delta S_{1 \rightarrow 2}^A$  for the  $0 \rightarrow 1$  and  $1 \rightarrow 2$  transition, respectively, as a function of magnetic field  $B_{\perp}$ . In Fig 3(a), upon increasing  $B_{\perp}$  the entropy change decreases from  $k_B \ln(2)$  to 0. This is in agreement with the two-fold degenerate ground state at zero magnetic field given by the Kramers pair  $|K^- \downarrow\rangle, |K^+ \uparrow\rangle$ . The degeneracy is gradually lifted with increasing  $B_{\perp}$  due to the spin- and valley-Zeeman effect: Once the energy splitting  $g_v \mu_B B_{\perp}$  between states  $|K^- \downarrow\rangle$  and  $|K^+ \uparrow\rangle$  exceeds the thermal energy  $k_B \bar{T}$ , the degeneracy is fully lifted in the thermodynamic sense, and the unambiguous thermodynamic ground state is  $|K^- \downarrow\rangle$ . Similar behaviour is also observed for the  $1 \rightarrow 2$ -transition in Fig 3(b) at magnetic fields below 100 mT: upon increasing  $B_{\perp}$  the entropy change increases from  $-k_B \ln(2)$  to 0 as the degeneracy of the one carrier state is lifted. Further increasing  $B_{\perp}$  leads to a peak in entropy change of  $k_B \ln(2)$  at 210 mT. Since here, the one-carrier ground state degeneracy is fully lifted already, the change in entropy must be fully due to a ground state degeneracy in the two-carrier charge state.

We compare the extracted entropy change in magnetic field with the energy level spectrum of the QD obtained from finite bias spectroscopy measurements performed in an out-of-plane magnetic which are shown in Fig. 3(c)-(d). For that we operate the QD into a regime where it is symmetrically coupled to two leads by adjusting the voltages of the barrier gates LB and RB. This is different from the regime in which the entropy measurements are performed, where the QD is only coupled to one lead, with the coupling controlled by RB. A source-drain bias  $V_{SD}$  is applied as well as a voltage modulation to the plunger gate PG in order to measure the transconductance  $\partial I_{\text{det}} / \partial V_{PG}$ . By carefully tuning the coupling to the leads, an excited state in the bias window increases the average occupation number of the dot, which expresses itself in the appearance of a peak in the transconductance. These peaks are labeled in Fig. 3 and identified according to the  $g$ -factors extracted. In Fig. 3(c) this is the Kramers pair  $|K^- \downarrow\rangle, |K^+ \uparrow\rangle$ , with the  $g$ -factors for the valley- and spin-Zeeman effects  $g_v^{(1)} = 14$  and  $g_s = 2$ , respectively, for the first hole carrier in the QD as well as the Kane-Mele spin-orbit gap  $\Delta_{SO} = 75 \mu\text{eV}$ .

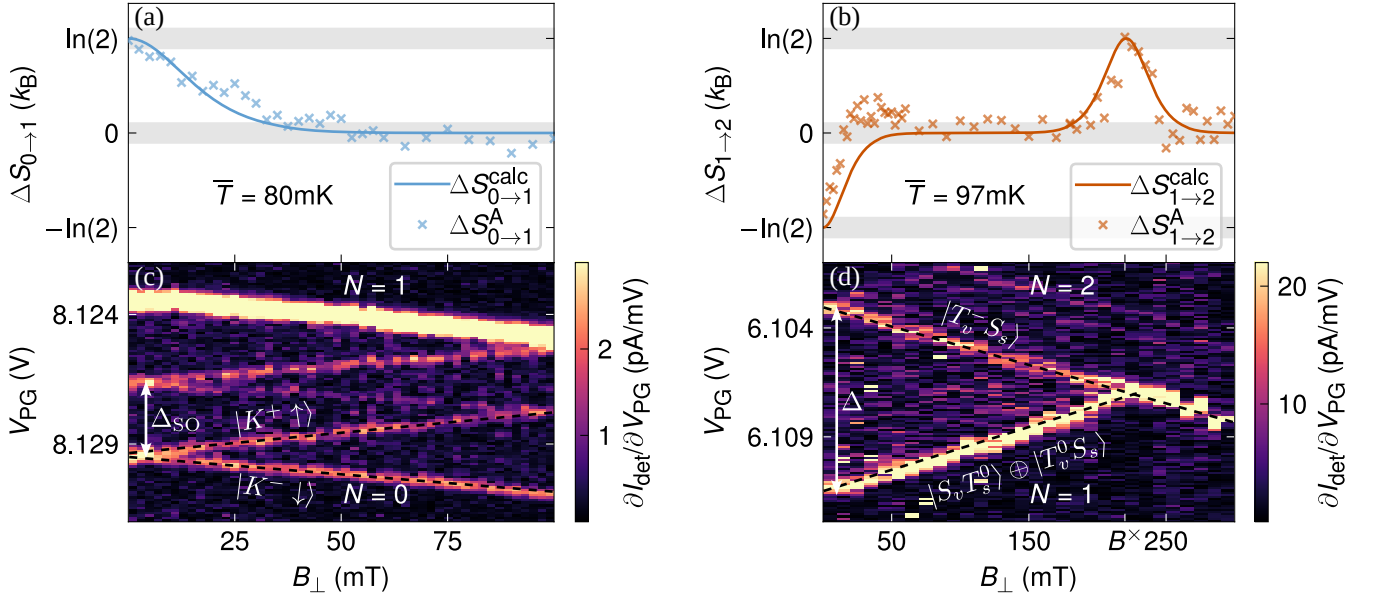


FIG. 3. Evolution of the measured entropy change in out-of-plane magnetic field together with the calculated entropy change (solid line) for the  $0 \rightarrow 1$  (a) and  $1 \rightarrow 2$  transition (b). for the  $0 \rightarrow 1$  and  $1 \rightarrow 2$  transitions. Finite bias spectroscopy measurements in out-of-plane magnetic field performed for the  $0 \rightarrow 1$  (c) and  $1 \rightarrow 2$  transition (d). The states are identified by there behaviour in out-of-plane magnetic field.

In Fig. 3(d) the ground state is labeled as  $|S_v T_s^0\rangle \oplus |T_v^0 S_s\rangle$ . Its energy does not change in out-of-plane magnetic field as there is no valley- or spin-Zeeman effect, as discussed in Sec. VI. The shift of the transconductance peak in magnetic field comes from the fact that the addition energy for the second carrier is affected by the energy of the first carrier. We observe a state crossing at 210 mT caused by a valley-triplet spin-singlet state labeled as  $|T_v^- S_s\rangle$ . Its energy gap to the ground state at zero-magnetic field is  $\Delta = 205 \mu\text{eV}$ . From the shift of the transconductance peak of  $|S_v T_s^0\rangle \oplus |T_v^0 S_s\rangle$  and  $|T_v^- S_s\rangle$ , the  $g$ -factor of the valley-Zeeman effect in the two carrier regime is found to be  $g_v^{(2)} = 16$ , supporting the proposed energy spectrum discussed in Sec. VI. Their values also agree with previous findings [33–35].

In the thermally broadened limit, the entropy evolution in magnetic field can be calculated. The calculation is carried out in Appendix D and results in expressions for  $\Delta S_{0 \rightarrow 1}^{\text{calc}}$  (eq. D32) and  $\Delta S_{1 \rightarrow 2}^{\text{calc}}$  (eq. D33). The corresponding traces are plotted in Figs. 3 (c) and (d). They show reasonable agreement with the measured entropy changes.

## VI. DISCUSSION & OUTLOOK

Measuring entropy allows us to directly determine the ground state degeneracy of charge states in a BLG QD. This approach gives insights beyond conventional transport spectroscopy techniques where degeneracies are detected in an indirect way by the energy levels splitting in magnetic field. The extracted entropy change for the

$0 \rightarrow 1$  transition is consistent with the excited state spectrum measured with finite bias spectroscopy and also previous findings [33, 34]: The ground state has a two-fold degeneracy (Kramers pair  $|K^- \downarrow\rangle, |K^+ \uparrow\rangle$ ) lifted in out-of-plane magnetic field due to the valley- and spin-Zeeman effect. For the  $1 \rightarrow 2$  transition the extracted entropy change reveals a non-degenerate ground state for the two-carrier charge state at zero magnetic field. This has not been observed before. Previous studies hinted towards a three-fold degenerate ground state given by a valley-singlet spin-triplet states [33, 34].

We attribute this finding to the effect of the Kane-Mele type spin-orbit interaction [36, 37] present in BLG and the exceptionally small exchange splitting between different valley states. A model is developed (Appendix B) with the resulting energy spectrum shown in Fig. 4. For the two-carrier charge state, the Kane-Mele type spin-orbit interaction leads to a coupling of the valley-singlet spin-triplet state  $|S_v T_s^0\rangle$  with the valley-triplet spin-singlet state  $|T_v^0 S_s\rangle$ . This results in the three-fold degeneracy being lifted. The new ground state is denoted as  $|S_v T_s^0\rangle \oplus |T_v^0 S_s\rangle$ . Its energy is lowered by

$$\Delta'_{\text{SO}} = \sqrt{\left(\frac{J_1 + J_2}{2}\right)^2 + \Delta_{\text{SO}}^2} - \frac{J_1 + J_2}{2} \quad (9)$$

compared to the valley-singlet spin-triplet states  $|S_v T_s^-\rangle, |S_v T_s^+\rangle$ . To give an estimate, we assume that  $J_1 \approx J_2$  and set  $J_1 = J_2 = \Delta = 205 \mu\text{eV}$  and  $\Delta_{\text{SO}} = 75 \mu\text{eV}$ . Previous experiments showed  $J_1, J_2 \simeq 1000 \mu\text{eV}$  [33]. This results in  $\Delta'_{\text{SO}} = 25 \mu\text{eV}$ . The extended data set on finite bias spectroscopy presented in Appendix C shows

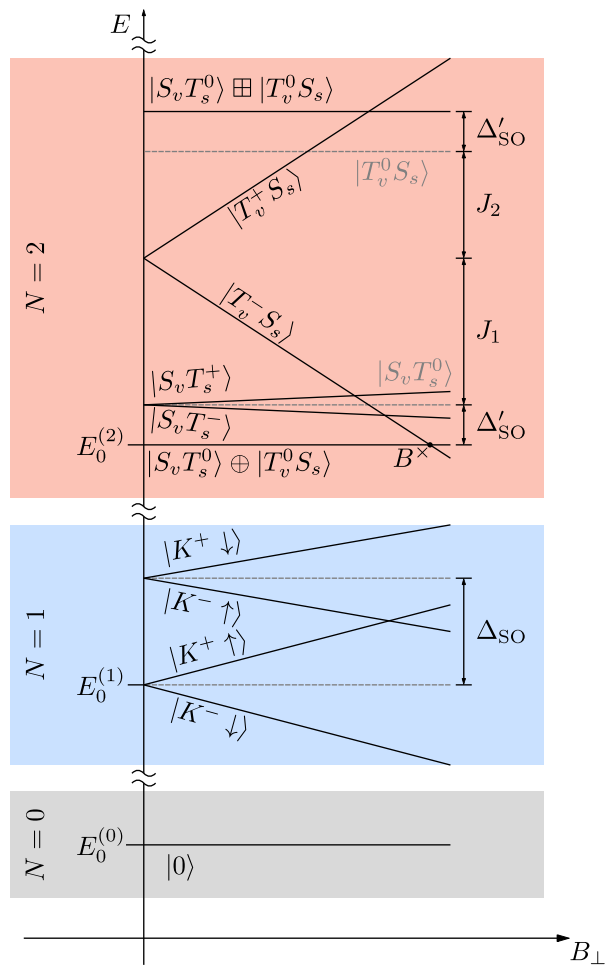


FIG. 4. Excited state spectra for the one-carrier and two-carrier state in an out-of-plane magnetic field including the effect of Kane-Mele type spin-orbit interaction for the  $N = 2$  charge state. The ground state  $|S_v T_s^0\rangle \oplus |T_v^0 S_s\rangle$  is separated from the spin-triplet states  $|S_v T_s^+\rangle$ ,  $|S_v T_s^-\rangle$  by an energy gap  $\Delta'_{SO}$ . The ground state crossing is due to the valley-triplet state  $|T_v^- S_s\rangle$  and appears at an out-of-plane magnetic field of  $B^x$ .

the presence of a gap between ground state and first excited state of roughly  $45 \mu\text{eV}$ . Furthermore, the energy of the first excited state in the two-carrier charge state shifts with a  $g$ -factor of 2, suggesting that it is indeed a spin-triplet state. The fact that entropy spectroscopy allows us to detect any residual degeneracies that are not lifted by magnetic field and that the resolution in energy is only limited by  $k_B T \approx 8 \mu\text{eV}$  make this method a valuable addition to conventional transport spectroscopy methods.

Our work generalizes and extends the Maxwell relation-based entropy measurements to samples fabricated in novel 2D vdW heterostructures and shows that sophisticated device designs can be implemented in these material systems, paving the way to probe various exotic states in BLG devices. Examples of these are the (multichannel-) Kondo effect [38, 39] or quantum spin chains with fractional or integer spins [40, 41].

## ACKNOWLEDGMENTS

We appreciate the many discussions with Josh Folk, Eran Sela, and Yigal Meir concerning the concept of entropy in mesoscopic systems. We thank Peter Märki, Thomas Böhler, as well as the FIRST staff for their technical support. We acknowledge support from the European Graphene Flagship Core3 Project, Swiss National Science Foundation via NCCR Quantum Science, and H2020 European Research Council (ERC) Synergy Grant under Grant Agreement 95154.

K.W. and T.T. acknowledge support from the JSPS KAKENHI (Grant Numbers 20H00354 and 23H02052) and World Premier International Research Center Initiative (WPI), MEXT, Japan.

- [1] N. R. Cooper and A. Stern, Observable Bulk Signatures of Non-Abelian Quantum Hall States, *Physical Review Letters* **102**, 176807 (2009).
- [2] G. Ben-Shach, C. R. Laumann, I. Neder, A. Yacoby, and B. I. Halperin, Detecting Non-Abelian Anyons by Charging Spectroscopy, *Physical Review Letters* **110**, 106805 (2013).
- [3] G. Viola, S. Das, E. Grosfeld, and A. Stern, Thermoelectric Probe for Neutral Edge Modes in the Fractional Quantum Hall Regime, *Physical Review Letters* **109**, 146801 (2012).
- [4] S. Smirnov, Majorana tunneling entropy, *Physical Review B* **92**, 195312 (2015).
- [5] C. Han, Z. Iftikhar, Y. Kleeorin, A. Anthore, F. Pierre, Y. Meir, A. K. Mitchell, and E. Sela, Fractional Entropy of Multichannel Kondo Systems from Conductance-Charge Relations, *Physical Review Letters* **128**, 146803 (2022).
- [6] B. A. Schmidt, K. Bennaceur, S. Gaucher, G. Gervais, L. N. Pfeiffer, and K. W. West, Specific heat and entropy of fractional quantum Hall states in the second Landau level, *Physical Review B* **95**, 201306 (2017).
- [7] Y. Kleeorin, H. Thierschmann, H. Buhmann, A. Georges, L. W. Molenkamp, and Y. Meir, How to measure the entropy of a mesoscopic system via thermoelectric transport, *Nature Communications* **10**, 5801 (2019).
- [8] N. Hartman, C. Olsen, S. Lüscher, M. Samani, S. Fallahi, G. C. Gardner, M. Manfra, and J. Folk, Direct entropy measurement in a mesoscopic quantum system, *Nature Physics* **14**, 1083 (2018).
- [9] E. Sela, Y. Oreg, S. Plugge, N. Hartman, S. Lüscher, and J. Folk, Detecting the Universal Fractional Entropy



- of Majorana Zero Modes, *Physical Review Letters* **123**, 147702 (2019).
- [10] T. Child, O. Sheekey, S. Lüscher, S. Fallahi, G. C. Gardner, M. Manfra, A. Mitchell, E. Sela, Y. Kleeorin, Y. Meir, and J. Folk, Entropy Measurement of a Strongly Coupled Quantum Dot, *Physical Review Letters* **129**, 227702 (2022).
- [11] T. Child, O. Sheekey, S. Lüscher, S. Fallahi, G. C. Gardner, M. Manfra, and J. Folk, A Robust Protocol for Entropy Measurement in Mesoscopic Circuits, *Entropy* **24**, 417 (2022).
- [12] C. Piquard, P. Glidic, C. Han, A. Aassime, A. Cavanna, U. Gennser, Y. Meir, E. Sela, A. Anthore, and F. Pierre, Observing the universal screening of a Kondo impurity, *Nature Communications* **14**, 7263 (2023).
- [13] Y. Cao, V. Fatemi, A. Demir, S. Fang, S. L. Tomarken, J. Y. Luo, J. D. Sanchez-Yamagishi, K. Watanabe, T. Taniguchi, E. Kaxiras, R. C. Ashoori, and P. Jarillo-Herrero, Correlated insulator behaviour at half-filling in magic-angle graphene superlattices, *Nature* **556**, 80 (2018).
- [14] M. Serlin, C. L. Tschirhart, H. Polshyn, Y. Zhang, J. Zhu, K. Watanabe, T. Taniguchi, L. Balents, and A. F. Young, Intrinsic quantized anomalous Hall effect in a moiré heterostructure, *Science* **367**, 900 (2020).
- [15] Y. Cao, V. Fatemi, S. Fang, K. Watanabe, T. Taniguchi, E. Kaxiras, and P. Jarillo-Herrero, Unconventional superconductivity in magic-angle graphene superlattices, *Nature* **556**, 43 (2018).
- [16] Y. Cao, D. Chowdhury, D. Rodan-Legrain, O. Rubies-Bigorda, K. Watanabe, T. Taniguchi, T. Senthil, and P. Jarillo-Herrero, Strange Metal in Magic-Angle Graphene with near Planckian Dissipation, *Physical Review Letters* **124**, 076801 (2020).
- [17] A. M. Seiler, F. R. Geisenhof, F. Winterer, K. Watanabe, T. Taniguchi, T. Xu, F. Zhang, and R. T. Weitz, Quantum cascade of correlated phases in trigonally warped bilayer graphene, *Nature* **608**, 298 (2022).
- [18] Y. Zhang, R. Polski, A. Thomson, E. Lantagne-Hurtubise, C. Lewandowski, H. Zhou, K. Watanabe, T. Taniguchi, J. Alicea, and S. Nadj-Perge, Enhanced superconductivity in spin-orbit proximitized bilayer graphene, *Nature* **613**, 268 (2023).
- [19] T. Han, Z. Lu, Y. Yao, J. Yang, J. Seo, C. Yoon, K. Watanabe, T. Taniguchi, L. Fu, F. Zhang, and L. Ju, Large quantum anomalous Hall effect in spin-orbit proximitized rhombohedral graphene, *Science* **384**, 647 (2024).
- [20] J. Vallejo Bustamante, N. J. Wu, C. Fermon, M. Pannetier-Lecoeur, T. Wakamura, K. Watanabe, T. Taniguchi, T. Pellegrin, A. Bernard, S. Daddinounou, V. Bouchiat, S. Guéron, M. Ferrier, G. Montambaux, and H. Bouchiat, Detection of graphene's divergent orbital diamagnetism at the Dirac point, *Science* **374**, 1399 (2021).
- [21] T. Arp, O. Sheekey, H. Zhou, C. L. Tschirhart, C. L. Patterson, H. M. Yoo, L. Holleis, E. Redekop, G. Babikyan, T. Xie, J. Xiao, Y. Vituri, T. Holder, T. Taniguchi, K. Watanabe, M. E. Huber, E. Berg, and A. F. Young, Intervalley coherence and intrinsic spin-orbit coupling in rhombohedral trilayer graphene, *Nature Physics* **20**, 1413 (2024).
- [22] Y. Zhang, T.-T. Tang, C. Girit, Z. Hao, M. C. Martin, A. Zettl, M. F. Crommie, Y. R. Shen, and F. Wang, Direct observation of a widely tunable bandgap in bilayer graphene, *Nature* **459**, 820 (2009).
- [23] C. H. Lui, Z. Li, K. F. Mak, E. Cappelluti, and T. F. Heinz, Observation of an electrically tunable band gap in trilayer graphene, *Nature Physics* **7**, 944 (2011).
- [24] E. McCann and M. Koshino, The electronic properties of bilayer graphene, *Reports on Progress in Physics* **76**, 056503 (2013).
- [25] F. Zhang, B. Sahu, H. Min, and A. H. MacDonald, Band structure of ABC-stacked graphene trilayers, *Physical Review B* **82**, 035409 (2010).
- [26] K. Hecker, L. Banszerus, A. Schäpers, S. Möller, A. Peters, E. Icking, K. Watanabe, T. Taniguchi, C. Volk, and C. Stampfer, Coherent charge oscillations in a bilayer graphene double quantum dot, *Nature Communications* **14**, 7911 (2023).
- [27] R. Garreis, C. Tong, J. Terle, M. J. Ruckriegel, J. D. Gerber, L. M. Gächter, K. Watanabe, T. Taniguchi, T. Ihn, K. Ensslin, and W. W. Huang, Long-lived valley states in bilayer graphene quantum dots, *Nature Physics* , 1 (2024).
- [28] A. O. Denisov, V. Reckova, S. Cances, M. J. Ruckriegel, M. Masseroni, C. Adam, C. Tong, J. D. Gerber, W. W. Huang, K. Watanabe, T. Taniguchi, T. Ihn, K. Ensslin, and H. Duprez, Ultra-long relaxation of a Kramers qubit formed in a bilayer graphene quantum dot (2024).
- [29] B. Huard, H. Pothier, D. Esteve, and K. E. Nagaev, Electron heating in metallic resistors at sub-Kelvin temperature, *Physical Review B* **76**, 165426 (2007).
- [30] E. Icking, L. Banszerus, F. Wörtche, F. Volmer, P. Schmidt, C. Steiner, S. Engels, J. Hesselmann, M. Goldsche, K. Watanabe, T. Taniguchi, C. Volk, B. Beschoten, and C. Stampfer, Transport Spectroscopy of Ultraclean Tunable Band Gaps in Bilayer Graphene, *Advanced Electronic Materials* **8**, 2200510 (2022).
- [31] A. Kurzmann, H. Overweg, M. Eich, A. Pally, P. Rickhaus, R. Pisoni, Y. Lee, K. Watanabe, T. Taniguchi, T. Ihn, and K. Ensslin, Charge Detection in Gate-Defined Bilayer Graphene Quantum Dots, *Nano Letters* **19**, 5216 (2019).
- [32] H. Duprez, S. Cances, A. Omahen, M. Masseroni, M. J. Ruckriegel, C. Adam, C. Tong, R. Garreis, J. D. Gerber, W. Huang, L. Gächter, K. Watanabe, T. Taniguchi, T. Ihn, and K. Ensslin, Spin-valley locked excited states spectroscopy in a one-particle bilayer graphene quantum dot, *Nature Communications* **15**, 9717 (2024).
- [33] A. Kurzmann, M. Eich, H. Overweg, M. Mangold, F. Herman, P. Rickhaus, R. Pisoni, Y. Lee, R. Garreis, C. Tong, K. Watanabe, T. Taniguchi, K. Ensslin, and T. Ihn, Excited States in Bilayer Graphene Quantum Dots, *Physical Review Letters* **123**, 026803 (2019).
- [34] S. Möller, L. Banszerus, A. Knothe, C. Steiner, E. Icking, S. Trellenkamp, F. Lentz, K. Watanabe, T. Taniguchi, L. Glazman, V. Fal'ko, C. Volk, and C. Stampfer, Probing Two-Electron Multiplets in Bilayer Graphene Quantum Dots, *Physical Review Letters* **127**, 256802 (2021).
- [35] C. Tong, R. Garreis, A. Knothe, M. Eich, A. Sacchi, K. Watanabe, T. Taniguchi, V. Fal'ko, T. Ihn, K. Ensslin, and A. Kurzmann, Tunable Valley Splitting and Bipolar Operation in Graphene Quantum Dots, *Nano Letters* **21**, 1068 (2021).
- [36] C. L. Kane and E. J. Mele, Quantum Spin Hall Effect in Graphene, *Physical Review Letters* **95**, 226801 (2005).
- [37] S. Konschuh, M. Gmitra, D. Kochan, and J. Fabian, The-

- ory of spin-orbit coupling in bilayer graphene, *Physical Review B* **85**, 115423 (2012).
- [38] A. Kurzmann, Y. Kleorin, C. Tong, R. Garreis, A. Knothe, M. Eich, C. Mittag, C. Gold, F. K. de Vries, K. Watanabe, T. Taniguchi, V. Fal'ko, Y. Meir, T. Ihn, and K. Ensslin, Kondo effect and spin-orbit coupling in graphene quantum dots, *Nature Communications* **12**, 6004 (2021).
- [39] R. M. Potok, I. G. Rau, H. Shtrikman, Y. Oreg, and D. Goldhaber-Gordon, Observation of the two-channel Kondo effect, *Nature* **446**, 167 (2007).
- [40] F. D. M. Haldane, Nonlinear Field Theory of Large-Spin Heisenberg Antiferromagnets: Semiclassically Quantized Solitons of the One-Dimensional Easy-Axis N\`eel State, *Physical Review Letters* **50**, 1153 (1983).
- [41] F. D. M. Haldane, Continuum dynamics of the 1-D Heisenberg antiferromagnet: Identification with the O(3) nonlinear sigma model, *Physics Letters A* **93**, 464 (1983).



## Appendix A: Sample Design

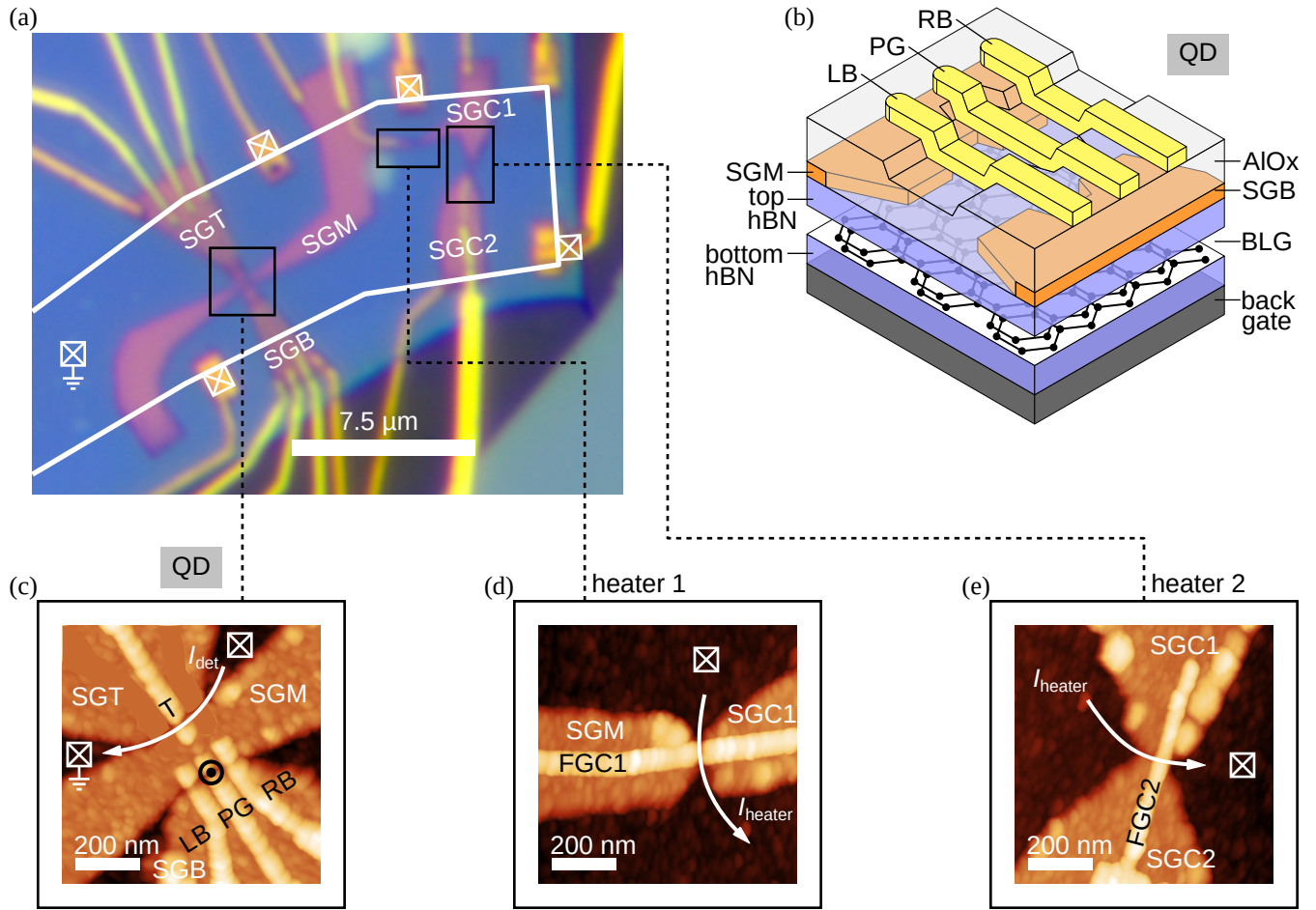


FIG. 5. (a) Optical microscope image of the used sample. The BLG flake is outlined in white. The applied back gate voltage is negative, rendering the BLG p-type/hole conducting. The split gate pairs SGM, SGB and SGM, SGT are used to electrostatically define a conducting channel. (b) Schematic of the VdW stack structure in the region where the QD is defined. AFM images of the (c) QD (black circles) formed with finger gates LB, PG, RB and the charge detector tuned with finger gate T, and the (d) (e) heater gate structures to form the ohmic constrictions, which are formed with split gates SGM, SGC1, SGC2 and finger gates FGC1 and FGC2.

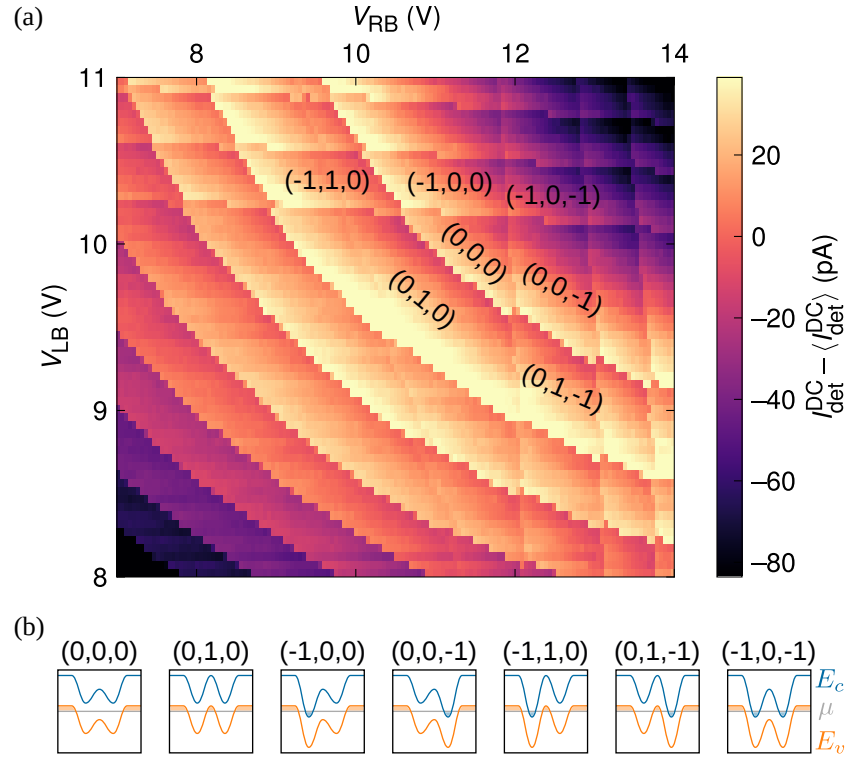


FIG. 6. (a) Charge detector current as a function of left and right barrier voltage. The plunger gate voltage is fixed to 3.25 V. Three types of resonances, corresponding to three types of QDs are observed: 1. pn-junction defined electron QD under LB corresponding to the horizontal transconductance peaks. 2. barrier defined hole QD between LB and RB corresponding to the bent transconductance peaks. This is the QD used for the entropy measurements. 3. pn-junction defined electron QD under RB corresponding to the vertical transconductance peaks. The number triplet labels the occupation number of the respective QDS (1., 2. 3.). (b) Diagrams showing the band bending induced by the finger gates LB, PG, RB in order to form the different types of QDs for a few exemplary cases. QDs form where the conduction band edge  $E_c$  or valence band edge  $E_v$  crosses the chemical potential  $\mu$  in energy.

## Appendix B: Excited state spectra for one & two carriers

Here, we put forward a model that captures the effect of Kane-Mele type SOI, as present in BLG, on the energy spectrum of the second charge carrier state. We assume that the carriers are in their orbital ground state. The valley quantum numbers are denoted as  $K^+$  (valley plus),  $K^-$  (valley minus), and the spin quantum numbers as  $\uparrow$  (spin up),  $\downarrow$  (spin down). We focus on the Hilbert space spanned by valley- and spin degree of freedom, i.e.  $\mathcal{H} = \mathcal{H}_v \otimes \mathcal{H}_s$ . One can form valley-singlet and -triplet states:

$$|S_v\rangle = \frac{1}{\sqrt{2}}(|K^+K^- \rangle - |K^-K^+ \rangle) \quad (\text{B1})$$

$$|T_v^-\rangle = |K^-K^-\rangle \quad (\text{B2})$$

$$|T_v^0\rangle = \frac{1}{\sqrt{2}}(|K^+K^- \rangle + |K^-K^+ \rangle) \quad (\text{B3})$$

$$|T_v^+\rangle = |K^+K^+\rangle \quad (\text{B4})$$

as well as spin-singlet and -triplet states:

$$|S_s\rangle = \frac{1}{\sqrt{2}}(|\uparrow\downarrow\rangle - |\downarrow\uparrow\rangle) \quad (\text{B5})$$

$$|T_s^-\rangle = |\downarrow\downarrow\rangle \quad (\text{B6})$$

$$|T_s^0\rangle = \frac{1}{\sqrt{2}}(|\uparrow\downarrow\rangle + |\downarrow\uparrow\rangle) \quad (\text{B7})$$

$$|T_s^+\rangle = |\uparrow\uparrow\rangle \quad (\text{B8})$$

The Hamiltonians operating in  $\mathcal{H}$  describing the one- and two-particle energy spectra are then given by

$$\mathcal{H}_{\text{ES}}^{(1)} = \begin{pmatrix} |K^- \downarrow\rangle & |K^+ \uparrow\rangle & |K^- \uparrow\rangle & |K^+ \downarrow\rangle \\ -\frac{1}{2}(g_v^{(1)} + g_s)\mu_B B_\perp & 0 & 0 & 0 \\ 0 & \frac{1}{2}(g_v^{(1)} + g_s)\mu_B B_\perp & 0 & 0 \\ 0 & 0 & \Delta_{\text{SO}} - \frac{1}{2}(g_v^{(1)} - g_s)\mu_B B_\perp & 0 \\ 0 & 0 & 0 & \Delta_{\text{SO}} + \frac{1}{2}(g_v^{(1)} - g_s)\mu_B B_\perp \end{pmatrix} \quad (\text{B9})$$

$$\mathcal{H}_{\text{ES}}^{(2)} = \begin{pmatrix} |S_v T_s^0\rangle & |S_v T_s^-\rangle & |S_v T_s^+\rangle & |S_s T_v^-\rangle & |S_s T_v^+\rangle & |S_s T_v^0\rangle \\ 0 & 0 & 0 & 0 & 0 & \Delta_{\text{SO}} \\ 0 & -g_s \mu_B B_\perp & 0 & 0 & 0 & 0 \\ 0 & 0 & g_s \mu_B B_\perp & 0 & 0 & 0 \\ 0 & 0 & 0 & J_1 - g_v^{(2)} \mu_B B_\perp & 0 & 0 \\ 0 & 0 & 0 & 0 & J_1 + g_v^{(2)} \mu_B B_\perp & 0 \\ \Delta_{\text{SO}} & 0 & 0 & 0 & 0 & J_1 + J_2 \end{pmatrix} \quad (\text{B10})$$

Diagonalization leads to the eigen states and -energies compiled in Tab. I and Tab. II. The spectrum is visualized in Fig. 7. The Kane-Mele SOI induced splitting between the new ground state and the first excited state of the two-carrier charge state is given by

$$\Delta'_{\text{SO}} = \sqrt{\left(\frac{J_1 + J_2}{2}\right)^2 + \Delta_{\text{SO}}^2} - \frac{J_1 + J_2}{2} > 0 \quad (\text{B11})$$

The angle  $\theta$  characteristic for the superposition that forms the new ground state is given by the relation

$$\tan(\theta) = \frac{2\Delta_{\text{SO}}}{J_1 + J_2} \quad (\text{B12})$$

From this one can see that the strength of mixing between states  $|S_v T_s^0\rangle$  and  $|T_v^0 S_s\rangle$  depends on how large the Kane-Mele spin-orbit gap  $\Delta_{\text{SO}}$  is compared to the exchange splittings  $J_1, J_2$ . For  $\Delta_{\text{SO}} \ll J_1 + J_2$  one obtains  $|S_v T_s^0\rangle$  as the ground state, whereas for  $\Delta_{\text{SO}} \gg J_1 + J_2$  the ground state is given by the superposition  $\frac{1}{\sqrt{2}}(|S_v T_s^0\rangle - |T_v^0 S_s\rangle)$ .

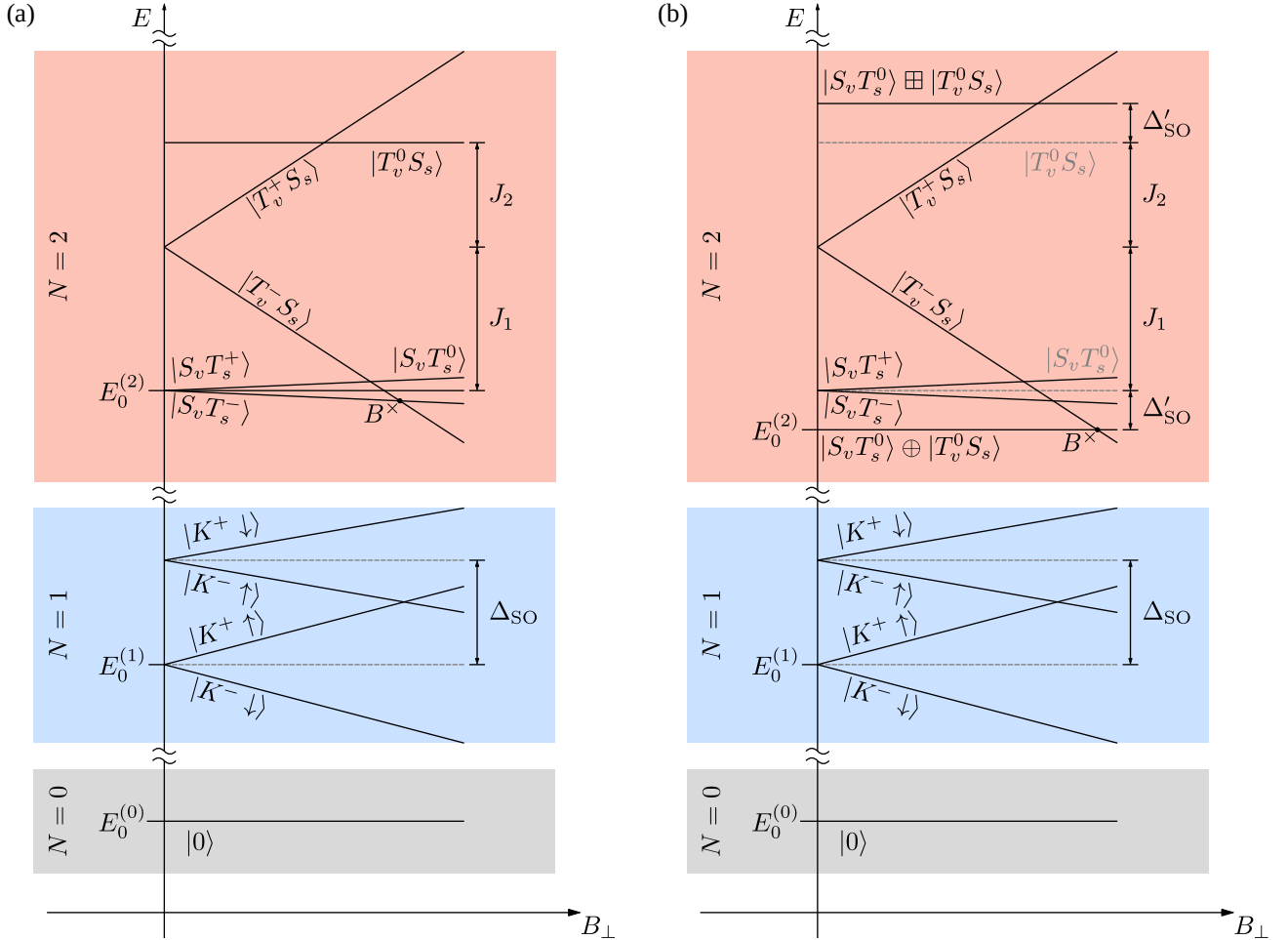
Applying an out-of-plane magnetic field  $B_\perp$  does not cause a change in ground state for the  $N = 0$  and  $N = 1$  charge carrier states. For the  $N = 2$  charge carrier state there is a ground state crossing happening at field  $B^\times$ . For  $B_\perp > B^\times$  the new ground state is given by  $|T_v^- S_s\rangle$ . Further increasing the magnetic field leads to higher orbital states coming down in energy. This is not shown in Fig. 7.

TABLE I. Excited state spectrum of the one-carrier charge state.

eigen states	eigen energies (w.r.t. $E_0^{(1)}$ )
$ K^- \downarrow\rangle$	$-\frac{1}{2}(g_v^{(1)} + g_s)\mu_B B_\perp$
$ K^+ \uparrow\rangle$	$+\frac{1}{2}(g_v^{(1)} + g_s)\mu_B B_\perp$
$ K^- \uparrow\rangle$	$\Delta_{\text{SO}} - \frac{1}{2}(g_v^{(1)} - g_s)\mu_B B_\perp$
$ K^+ \downarrow\rangle$	$\Delta_{\text{SO}} + \frac{1}{2}(g_v^{(1)} - g_s)\mu_B B_\perp$

TABLE II. Excited state spectrum of the two-carrier charge state.

eigen states	eigen energies (w.r.t. $E_0^{(2)}$ )
$\cos(\frac{\theta}{2}) S_v T_s^0\rangle - \sin(\frac{\theta}{2}) T_v^0 S_s\rangle$ $=:  S_v T_s^0\rangle \oplus  T_v^0 S_s\rangle$	0
$ S_v T_s^-\rangle$	$\Delta'_{\text{SO}} - g_s \mu_B B_\perp$
$ S_v T_s^0\rangle$	$\Delta'_{\text{SO}}$
$ S_v T_s^+\rangle$	$\Delta'_{\text{SO}} + g_s \mu_B B_\perp$
$ S_s T_v^-\rangle$	$\Delta'_{\text{SO}} + J_1 - g_v^{(2)} \mu_B B_\perp$
$ S_s T_v^+\rangle$	$\Delta'_{\text{SO}} + J_1 + g_v^{(2)} \mu_B B_\perp$
$ S_s T_v^0\rangle$	$\Delta'_{\text{SO}} + J_1 + J_2$
$\sin(\frac{\theta}{2}) S_v T_s^0\rangle + \cos(\frac{\theta}{2}) T_v^0 S_s\rangle$ $=:  S_v T_s^0\rangle \boxplus  T_v^0 S_s\rangle$	$2\Delta'_{\text{SO}} + J_1 + J_2$

FIG. 7. Energy spectrum without (a) and with (b) considering the effect of Kane-Mele type SOI for the two-carrier charge state  $N = 2$ .

## Appendix C: Finite bias spectroscopy

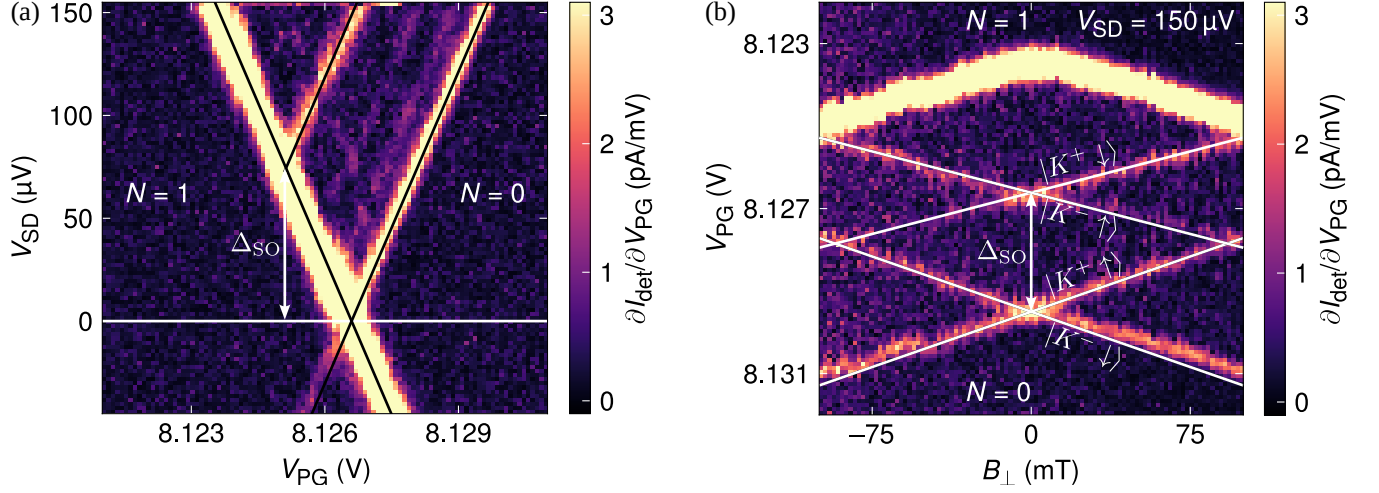


FIG. 8. (a) Coulomb diamond measurement at the  $1 \rightarrow 2$ -transition. The transconductance peaks show the ground state and an excited state separated in energy  $\Delta_{\text{SO}}$  from the ground state. The lever arm for the first carrier is extracted from this measurement. (b) Finite bias measurement in out-of-plane magnetic field. The ground state splits into two states, the Kramers pair  $|K^- \downarrow\rangle$ ,  $|K^+ \uparrow\rangle$ . The excited state splits into the Kramers pair  $|K^- \uparrow\rangle$ ,  $|K^+ \downarrow\rangle$ . From the slopes we extract the  $g$ -factors for the valley-  $g_v^{(1)}$  and spin-Zeeman effect  $g_s^{(1)}$  for the first carrier. All extracted parameters are compiled in Tab. III.

TABLE III. Parameters from  $0 \rightarrow 1$  transition

lever arm	$\alpha_{\text{PG}}^{(1)} = 0.025$
SO splitting	$\Delta_{\text{SO}} = 73 \mu\text{eV}$
valley $g$ -factor	$g_v^{(1)} = 13.6$
spin $g$ -factor	$g_s^{(1)} = 2.0$

TABLE IV. Parameters from  $1 \rightarrow 2$  transition

leverarm	$\alpha_{\text{PG}}^{(2)} = 0.025$
SO induced splitting	$\Delta_{\text{SO}} = 45 \mu\text{eV}$
exchange splitting	$J_1 = 160 \mu\text{eV}$
valley $g$ -factors first carrier	$g_v^{(1)} = 15.5$
valley $g$ -factor second carrier	$g_v^{(2)} = 16.0$
spin $g$ -factor	$g_s^{(2)} = 2.0$

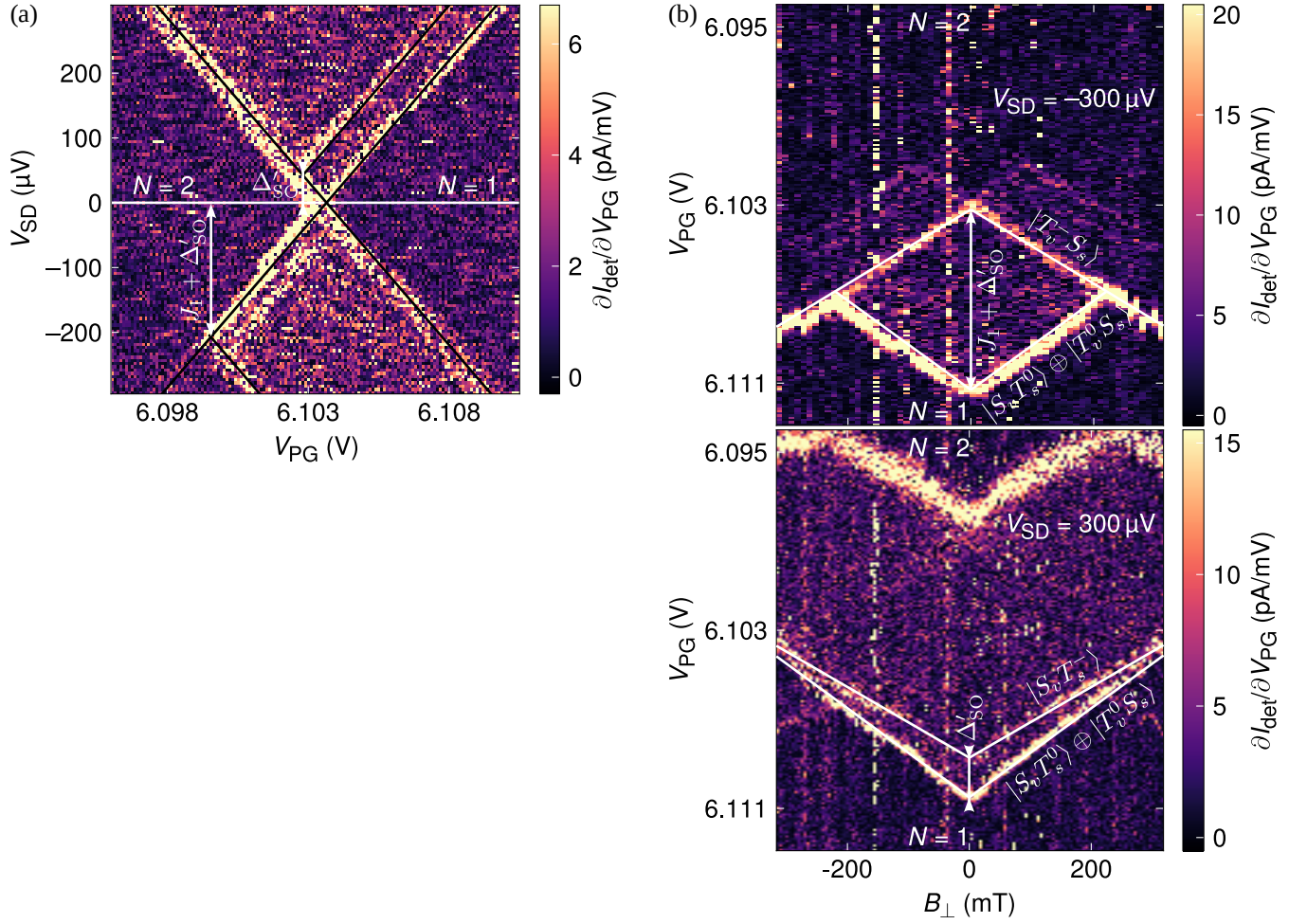


FIG. 9. (a) Coulomb diamond measurement at the  $1 \rightarrow 2$ -transition. The transconductance peaks show the ground state and two excited states: one for positive bias separated by the energy  $\Delta'_{SO}$  from the ground state, one for negative bias separated by the energy  $\Delta'_{SO} + J_1$  from the ground state. The lever arm for the first carrier is extracted from this measurement. (b) Finite bias measurement in out-of-plane magnetic field. The ground state does not split. The excited state with energy separation of  $\Delta'_{SO}$  only visible for positive bias moves down in energy with a  $g$ -factor of 2.0, indicating that it is the state  $|S_v T_s^- \rangle$ . The excited state with an energy separation of  $\Delta'_{SO} + J_1$  only visible for negative bias moves down in energy with a  $g$ -factor of 16.0, indicating that it is the state  $|S_v T_s^- \rangle$ . All extracted parameters are compiled in Tab. IV.

## Appendix D: Thermodynamic Model

### 1. Grand canonical ensemble

QD is coupled to a reservoir, allowing for carrier and energy to fluctuate. If the coupling is dominated by thermal broadening, i.e.  $k_B T \gg \Gamma_R$ , the thermodynamics of the system is in general described in the framework of the grand canonical ensemble. The grand partition function is given by

$$\mathcal{Z}(\mu, T) = \sum_{N=0}^{\infty} \sum_{i=0}^{\infty} e^{-\frac{E_i^{(N)} - N\mu}{k_B T}} \quad (\text{D1})$$

$$= \sum_{N=0}^{\infty} e^{-\frac{E_0^{(N)} - N\mu}{k_B T}} \sum_{i=0}^{\infty} e^{-\frac{\Delta_i^{(N)}}{k_B T}} \quad (\text{D2})$$

where we introduced the decomposition

$$E_i^{(N)} = E_0^{(N)} + \Delta_i^{(N)} \quad (\text{D3})$$

where  $E_i^{(N)}$  is the energy of the  $i$ th excited state of the  $N$ -charge carrier state,  $E_0^{(N)}$  the ground state energy of the  $N$ -charge carrier state, and  $\Delta_i^{(N)}$  the energy difference between the respective excited state and the ground state. All macroscopic state quantities such as  $\bar{N}(\mu, T)$  and  $S(\mu, T)$  can be calculated from  $\mathcal{Z}(\mu, T)$ , as well as the occupation probability  $p_i^{(N)}(\mu, T)$  of the microstate labeled  $(N, i)$ . In terms of  $\mathcal{Z}(\mu, T)$  one finds

$$p_i^{(N)}(\mu, T) = -k_B T \frac{\partial \ln \mathcal{Z}(\mu, T)}{\partial E_i^{(N)}} \quad (\text{D4})$$

$$\bar{N}(\mu, T) = k_B T \frac{\partial \ln \mathcal{Z}(\mu, T)}{\partial \mu} \quad (\text{D5})$$

$$S(\mu, T) = k_B \ln \mathcal{Z}(\mu, T) + k_B T \frac{\partial \ln \mathcal{Z}(\mu, T)}{\partial T} . \quad (\text{D6})$$

and in terms of microstates/microstate probabilities one has

$$p_i^{(N)}(\mu, T) = \frac{e^{-\frac{E_0^{(N)} - N\mu}{k_B T}}}{\mathcal{Z}(\mu, T)} e^{-\frac{\Delta_i^{(N)}}{k_B T}} \quad (\text{D7})$$

$$\bar{N}(\mu, T) = \sum_{N=0}^{\infty} N \sum_{i=0}^{\infty} p_i^{(N)}(\mu, T) \quad (\text{D8})$$

$$S(\mu, T) = -k_B \sum_{N=0}^{\infty} \sum_{i=0}^{\infty} p_i^{(N)} \ln(p_i^{(N)}) \quad (\text{D9})$$

### 2. Entropy at zero magnetic field

For the charge transition  $N - 1 \leftrightarrow N$  contributions of other charge states can be neglected if  $k_B T \ll E_0^{(N-1)} - E_0^{(N-2)}$ ,  $E_0^{(N+1)} - E_0^{(N)}$ . The grand partition function becomes

$$\mathcal{Z}^{(N-1 \leftrightarrow N)}(\mu, T) = e^{-\frac{E_0^{(N-1)} - (N-1)\mu}{k_B T}} \sum_{i=0}^{\infty} e^{-\frac{\Delta_i^{(N-1)}}{k_B T}} + e^{-\frac{E_0^{(N)} - N\mu}{k_B T}} \sum_{i=0}^{\infty} e^{-\frac{\Delta_i^{(N)}}{k_B T}} \quad (\text{D10})$$

If additionally  $k_B T \ll \Delta_i^{(N)}$ ,  $\Delta_i^{(N-1)}$  one can also neglect excited states of the respective charge state in the expression for the grand partition function. Under these considerations, the grand partition function, the microstate probabilities, and the entropy are for the  $0 \rightarrow 1$ -transition given by



$$\mathcal{Z}^{(0\leftrightarrow 1)} = e^{-\frac{E_0^{(0)}}{k_B T}} + e^{-\frac{E_0^{(1)} - \mu}{k_B T}} \cdot 2 \quad (\text{D11})$$

$$p_0^{(0)} = \frac{1}{1 + e^{-\frac{\mu_0^{(1)} - \mu}{k_B T} + \ln(2)}} \quad (\text{D12})$$

$$p_{|K^-\downarrow}^{(1)} = p_{|K^+\uparrow}^{(1)} = \frac{1}{2} \frac{1}{1 + e^{\frac{\mu_0^{(1)} - \mu}{k_B T} - \ln(2)}} \quad (\text{D13})$$

$$S^{(0\leftrightarrow 1)} = -k_B \left[ p_0^{(0)} \ln(p_0^{(0)}) + p_{|K^-\downarrow}^{(1)} \ln(p_{|K^-\downarrow}^{(1)}) + p_{|K^+\uparrow}^{(1)} \ln(p_{|K^+\uparrow}^{(1)}) \right] \quad (\text{D14})$$

and for the  $1 \rightarrow 2$ -transition

$$\mathcal{Z}^{(1\leftrightarrow 2)} = e^{-\frac{E_0^{(1)} - \mu}{k_B T}} \cdot 2 + e^{-\frac{E_0^{(2)} - 2\mu}{k_B T}} \quad (\text{D15})$$

$$p_{|K^-\downarrow}^{(1)} = p_{|K^+\uparrow}^{(1)} = \frac{1}{2} \frac{1}{1 + e^{-\frac{\mu_0^{(2)} - \mu}{k_B T} - \ln(2)}} \quad (\text{D16})$$

$$p_{|S_v T_s^0 \oplus |T_v^0 S_s}^{(2)} = \frac{1}{1 + e^{\frac{\mu_0^{(2)} - \mu}{k_B T} + \ln(2)}} \quad (\text{D17})$$

$$S^{(1\leftrightarrow 2)} = -k_B \left[ p_{|K^-\downarrow}^{(1)} \ln(p_{|K^-\downarrow}^{(1)}) + p_{|K^+\uparrow}^{(1)} \ln(p_{|K^+\uparrow}^{(1)}) + p_{|S_v T_s^0 \oplus |T_v^0 S_s}^{(2)} \ln(p_{|S_v T_s^0 \oplus |T_v^0 S_s}^{(2)}) \right] \quad (\text{D18})$$

Note that here the kets merely serve as labels. Only the ground state degeneracies of the respective charge states and the temperature determine the line shape of these functions.

### 3. Entropy at fixed particle number $N$

By putting the chemical potential  $\mu$  far away from any transition, the particle number  $N$  is fixed. The QD is in the  $N$  carrier state with absolute certainty. A description in the canonical ensemble framework is appropriate. The partition function is then given by

$$Z^{(N)}(T) = \sum_{j=0}^{\infty} e^{-\frac{\Delta_j^{(N)}}{k_B T}} \quad (\text{D19})$$

The probabilities of the microstates being realized is

$$p_i^{(N)}(T) = \frac{e^{-\frac{\Delta_i^{(N)}}{k_B T}}}{\sum_{j=0}^{\infty} e^{-\frac{\Delta_j^{(N)}}{k_B T}}} \quad (\text{D20})$$

### 4. Microstate probabilities of the BLG QD

For the  $N = 0$  carrier state we find

$$Z^{(0)} = 1 \quad (\text{D21})$$

$$p_0^{(0)} = 1 \quad (\text{D22})$$

$$S_0 = 0 \quad (\text{D23})$$

With Tab. I we find for the  $N = 1$  carrier state

$$Z^{(1)} = e^{\frac{(g_v^{(1)} + g_s)\mu_B B_\perp}{2k_B T}} + e^{\frac{(g_v^{(1)} + g_s)\mu_B B_\perp}{2k_B T}} \quad (\text{D24})$$

$$p_{|K-\downarrow}^{(1)} = \frac{e^{\frac{(g_v^{(1)} + g_s)\mu_B B_\perp}{2k_B T}}}{Z^{(1)}} \quad (\text{D25})$$

$$p_{|K+\uparrow}^{(1)} = \frac{e^{-\frac{(g_v^{(1)} + g_s)\mu_B B_\perp}{2k_B T}}}{Z^{(1)}} \quad (\text{D26})$$

$$S_1 = -k_B \left[ p_{|K-\downarrow}^{(1)} \ln(p_{|K-\downarrow}^{(1)}) + p_{|K+\uparrow}^{(1)} \ln(p_{|K+\uparrow}^{(1)}) \right] \quad (\text{D27})$$

where we included only the states lowest in energy as  $\Delta_{\text{SO}} > 4k_B T$  in the experiments. For the  $N = 2$  carrier state we find with Tab. II:

$$Z^{(2)} = 1 + e^{-\frac{\Delta'_{\text{SO}} + J_1 - g_v^{(2)}\mu_B B_\perp}{k_B T}} \quad (\text{D28})$$

$$p_{|S_v T_s^0 \oplus |T_v^0 S_s}^{(2)} = \frac{1}{Z^{(2)}} \quad (\text{D29})$$

$$p_{|T_v^- S_s}^{(2)} = \frac{e^{-\frac{\Delta'_{\text{SO}} + J_1 - g_v^{(1)}\mu_B B_\perp}{k_B T}}}{Z^{(2)}} \quad (\text{D30})$$

$$S_2 = -k_B \left[ p_{|S_v T_s^0 \oplus |T_v^0 S_s}^{(2)} \ln(p_{|S_v T_s^0 \oplus |T_v^0 S_s}^{(2)}) + p_{|T_v^- S_s}^{(2)} \ln(p_{|T_v^- S_s}^{(2)}) \right] \quad (\text{D31})$$

where we included only the states lowest in energy as  $\Delta'_{\text{SO}} > 4k_B T$  and states causing a ground state crossing at finite  $B_\perp$ . With these expressions we define

$$\Delta S_{0 \rightarrow 1}^{\text{calc}} = S_1 - S_0 \quad (\text{D32})$$

$$\Delta S_{1 \rightarrow 2}^{\text{calc}} = S_2 - S_1 \quad (\text{D33})$$